

# One Proximate Kitaev Spin Liquid in the $K$ - $J$ - $\Gamma$ Model on the Honeycomb Lattice

Jiucui Wang,<sup>1</sup> B. Normand,<sup>2</sup> and Zheng-Xin Liu<sup>1,\*</sup>

<sup>1</sup>*Department of Physics, Renmin University of China, Beijing 100872, China*

<sup>2</sup>*Neutrons and Muons Research Division, Paul Scherrer Institute, CH-5232 Villigen-PSI, Switzerland*  
(Dated: November 14, 2019)

In addition to the Kitaev ( $K$ ) interaction, candidate Kitaev materials also possess Heisenberg ( $J$ ) and off-diagonal symmetric ( $\Gamma$ ) couplings. We investigate the quantum ( $S = 1/2$ )  $K$ - $J$ - $\Gamma$  model on the honeycomb lattice by a variational Monte Carlo (VMC) method. In addition to the “generic” Kitaev spin liquid (KSL), we find that there is just one proximate KSL (PKSL) phase, while the rest of the phase diagram contains different magnetically ordered states. The PKSL is a gapless  $Z_2$  state with 14 Majorana cones, which in contrast to the KSL has a gapless spin response. In a magnetic field applied normal to the honeycomb plane, it realizes two of Kitaev’s gapped chiral spin-liquid phases, of which one is non-Abelian with Chern number  $\nu = 5$  and the other is Abelian with  $\nu = 4$ . These two phases could be distinguished by their thermal Hall conductance.

The Kitaev model [1] of bond-dependent Ising-type spin interactions on the honeycomb lattice offers exactly soluble examples of both gapped and gapless quantum spin liquids (QSLs). The magnetically disordered ground states of different QSLs are the consequence of strong intrinsic quantum fluctuations and provide particularly clean realizations of different fundamental phenomena. The gapped Kitaev QSL has  $Z_2$  Abelian topological order, while the quintessential “Kitaev spin liquid” (KSL) is the gapless state whose low-energy excitations form two Majorana cones, whereas its  $Z_2$  flux excitations are gapped. In an applied magnetic field, the Majorana cones become gapped and the resulting state is a chiral spin liquid (CSL) with Ising-type non-Abelian anyonic excitations, which have potential application in fault-tolerant topological quantum computation.

Thus the experimental realization of the Kitaev model has moved to the forefront of research in strongly correlated materials. While transition-metal compounds with strong spin-orbit coupling do realize Kitaev-type interactions [2, 3], these “candidate Kitaev” materials typically possess in addition significant non-Kitaev interactions, which lead to  $\text{Na}_2\text{IrO}_3$  [4, 5] and  $\alpha\text{-RuCl}_3$  [6–9] exhibiting magnetic order at low temperatures. Although  $\text{H}_3\text{LiIr}_2\text{O}_6$  [10] is not ordered, it appears to show strong impurity and extrinsic disordering effects. At the same order in a strong-coupling treatment [11], the Kitaev ( $K$ ) interaction is accompanied by Heisenberg ( $J$ ) and off-diagonal symmetric ( $\Gamma$ ) interactions, and thus the focus of the field has become the understanding of “proximate Kitaev” physics in this class of model, also under applied magnetic fields [12–15] and pressures [16].

In this Letter, we investigate the  $K$ - $J$ - $\Gamma$  extended Kitaev model by variational Monte Carlo (VMC) studies of a spinon representation. Guided by the projective symmetry group (PSG), we obtain the global  $K$ - $J$ - $\Gamma$  phase diagram and show that it contains two distinct QSL phases among several classically ordered phases. One QSL, at small  $J$  and  $\Gamma$ , is the generic KSL. At larger  $\Gamma$  we find one proximate KSL (PKSL), a non-Kitaev QSL sharing

the same PSG as the KSL but with 14 Majorana cones in the first Brillouin zone and gapless spin excitations. In an applied  $\hat{c}$ -axis field, all 14 cones are gapped and the PKSL hosts two exotic CSL phases, one with non-Abelian anyons and one with Abelian anyons. These results shed crucial new light on the parameter-space constraints and (induced) spin-liquid phases of candidate Kitaev materials.

In the candidate materials known to date,  $K < 0$  is believed to be ferromagnetic [17–20], while  $J$  has been argued to have both signs and extended nature, but all studies of the  $\Gamma$  (and  $\Gamma'$ ) term(s) take  $\Gamma > 0$  [21, 22]. The role of  $\Gamma$  in a fully quantum model remains little studied [23], but from classical models  $\Gamma$  is thought to explain the strongly anisotropic field response of  $\alpha\text{-RuCl}_3$  [8, 21]. In general, it is not yet accepted that a  $J = 0$  (i.e.  $K$ - $\Gamma$ ) model can support a magnetically ordered ground state [21], and it has been claimed on the basis of exact diagonalization of small systems [11, 24] and iDMRG studies of narrow cylinders [25] that multiple QSL phases may exist in the  $K$ - $J$ - $\Gamma$  model at small  $J$ .

The model we consider is

$$H = \sum_{\langle i,j \rangle \in \gamma} K S_i^\gamma S_j^\gamma + J \vec{S}_i \cdot \vec{S}_j + \Gamma (S_i^\alpha S_j^\beta + S_i^\beta S_j^\alpha), \quad (1)$$

where  $\langle i, j \rangle$  denotes nearest-neighbor sites and  $\gamma$  both the bond type on the honeycomb lattice and the spin index. Due to the spin-orbit coupling, the symmetry group of the model,  $G = D_{3d} \times Z_2^T$  where  $Z_2^T = \{E, T\}$  is time reversal, is finite, i.e. its elements are discrete operations combining the space-time and spin degrees of freedom.

We find the ground state of the  $S = 1/2$   $K$ - $J$ - $\Gamma$  model by VMC, which is a powerful method for the study of spin-liquid phases. We first introduce the fermionic slave-particle representation  $S_i^m = \frac{1}{2} C_i^\dagger \sigma^m C_i$ , where  $C_i^\dagger = (c_{i\uparrow}^\dagger, c_{i\downarrow}^\dagger)$ ,  $m \equiv x, y, z$ , and  $\sigma^m$  are Pauli matrices. The particle-number constraint,  $\hat{N}_i = c_{i\uparrow}^\dagger c_{i\uparrow} + c_{i\downarrow}^\dagger c_{i\downarrow} = 1$ , should be imposed at every site to ensure that the size of the fermion Hilbert space is the same as that of the

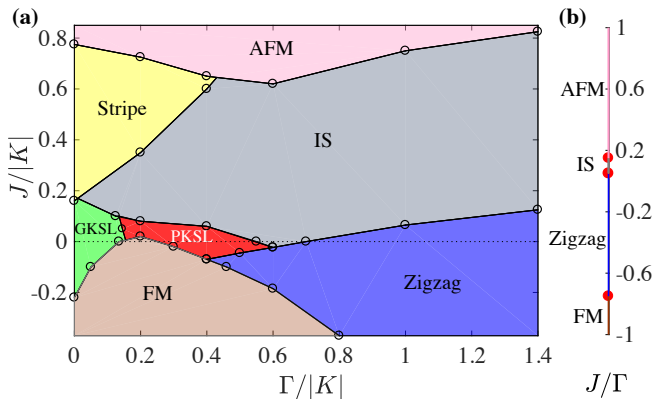


FIG. 1. (a) Phase diagram of the quantum  $K$ - $J$ - $\Gamma$  model for  $K < 0$  in the limit of large system size. There are two QSL phases of different types but with the same PSG, the GKSL and the PKSL. The magnetically ordered phases are antiferromagnetic (AFM), stripe, incommensurate spiral (IS), zigzag, and ferromagnetic (FM) order. (b) Detail of the limit  $|K|/\Gamma \rightarrow 0$ , where all phases are magnetically ordered; the transitions occur at  $J/\Gamma = 0.15, 0.05$ , and  $-0.75$ .

physical spin. This complex fermion representation is equivalent to the Majorana representation introduced by Kitaev [1]. It has a local  $SU(2)$  symmetry that is independent of the  $SU(2)$  spin-rotation operations and can be considered as a gauge structure [26], as discussed in Sec. S1A of the Supplemental Material (SM) [27]. The spin interactions in Eq. (1) are rewritten in terms of interacting fermionic operators and decoupled into a non-interacting mean-field Hamiltonian (Sec. S1B of the SM [27]), which for the most general spin-orbit-coupled spin liquid has the form

$$H_{\text{mf}} = \sum_{\langle i,j \rangle \in \gamma} \text{Tr} [U_{ji}^{(0)} \psi_i^\dagger \psi_j] + \text{Tr} [U_{ji}^{(1)} \psi_i^\dagger (iR_{\alpha\beta}^\gamma) \psi_j] \\ + \text{Tr} [U_{ji}^{(2)} \psi_i^\dagger \sigma^\gamma \psi_j] + \text{Tr} [U_{ji}^{(3)} \psi_i^\dagger \sigma^\gamma R_{\alpha\beta}^\gamma \psi_j], \quad (2)$$

where  $\psi_i = (C_i \bar{C}_i)$ ,  $\bar{C}_i = (c_{i\downarrow}^\dagger, -c_{i\uparrow}^\dagger)^T$ ,  $R_{\alpha\beta}^\gamma = -\frac{i}{\sqrt{2}}(\sigma^\alpha + \sigma^\beta)$  is a rotation matrix, and the quantities  $U_{ji}^{(m)}$ , with  $\gamma$  specified by  $\langle i, j \rangle$ , are mean-field parameters.

In the states described by Eq. (2), the  $SU(2)$  gauge symmetry is usually reduced to  $U(1)$  or  $Z_2$ , which is known as the invariant gauge group (IGG) [35]. The Majorana mean-field solution of the Kitaev model has IGG  $Z_2$ . Because the KSL is a special (exactly soluble) point in the model of Eq. (1), one expects a finite regime of QSL states connected adiabatically to it; following Ref. [36] we call this the generic KSL (GKSL). A QSL ground state preserves the full symmetry group,  $G$ , and so does the mean-field Hamiltonian. However, a general symmetry operation of this Hamiltonian is a space-time and spin operation in  $G$  combined with an  $SU(2)$  gauge transformation. These new symmetry operations form a larger group, known as the PSG, which is equivalent to a central extension of  $G$  by the IGG (Sec. S2

of the SM [27]). The PSG of the KSL is known exactly [37] and the corresponding mean-field Hamiltonian must respect it. The PSG reduces the number of independent parameters and, as detailed in Sec. S3 of the SM [27], the coefficients  $U_{ji}^{(m)}$  in Eq. (2) are constrained to the forms  $U_{ji}^{(0)} = i\eta_0 + i(\rho_a + \rho_c)$ ,  $U_{ji}^{(1)} = i(\rho_a - \rho_c + \rho_d)(\tau^\alpha + \tau^\beta) + i\eta_3(\tau^x + \tau^y + \tau^z)$ ,  $U_{ji}^{(2)} = i(\rho_a + \rho_c)\tau^\gamma + i\eta_5(\tau^x + \tau^y + \tau^z)$ , and  $U_{ji}^{(3)} = i(\rho_c - \rho_a - \rho_d)(\tau^\alpha - \tau^\beta)$ .

In addition we allow competing magnetically ordered phases by including the term  $H'_{\text{mf}} = \frac{1}{2} \sum_i \mathbf{M}_i \cdot C_i^\dagger \boldsymbol{\sigma} C_i$  in the mean-field Hamiltonian [23]. The ordering pattern of  $\mathbf{M}_i$  is set from the classical solution within the single- $\mathbf{Q}$  approximation, leaving only the amplitude,  $M$ , and the canting angle,  $\phi$ , to be determined variationally (Sec. S3 of the SM [27]). The power of the VMC approach is that it allows the particle-number constraint to be enforced locally, by performing Gutzwiller projection of the mean-field ground states to obtain the trial wave functions  $|\Psi(x)\rangle = P_G |\Psi_{\text{mf}}(x)\rangle$ , where  $x$  denotes the variational parameters  $(\rho_a, \rho_c, \rho_d, \eta_0, \eta_3, \eta_5, M, \phi)$ . These are determined by minimizing the trial ground-state energy,  $E(x) = \langle \Psi(x) | H | \Psi(x) \rangle / \langle \Psi(x) | \Psi(x) \rangle$ , in calculations performed on tori of up to  $14 \times 14$  unit cells, i.e. 392 lattice sites. Because the final variational states depend crucially on the mean-field Hamiltonian, a meaningful VMC procedure requires a careful choice and comparison of decoupling channels, and we have tested many spin-liquid and magnetic ansatzes (Sec. S3).

Figure 1 shows the VMC phase diagram of the  $K$ - $J$ - $\Gamma$  model at zero applied field. As a benchmark, we note that our phase boundaries at  $\Gamma = 0$ ,  $J > 0$  agree quantitatively with those of Ref. [38]. Although the mean-field phase diagram contains a number of candidate QSLs, VMC calculations reveal that only two are robust. One is the GKSL, whose regime of stability is bounded approximately by  $|J/K| = 0.2$  at  $\Gamma = 0$  and  $\Gamma/|K| = 0.15$ ; this result provides a quantitative statement of the region of relevance for the considerations of Ref. [36]. The second we name the PKSL, one of our central results being that there is only one QSL proximate to the GKSL. The GKSL and PKSL have the same PSG despite being physically quite different states. In contrast to the spinon excitation spectrum of the GKSL, which has two Majorana cones in the first Brillouin zone [Fig. 2(a)], the PKSL has 14 [Figs. 2(b) and 2(d)]. These cones are protected from local perturbations by the combination of spatial-inversion and time-reversal symmetry, as detailed in Sec. S3 of the SM [27]. We discuss the nature of the cones and the magnetic response of the PKSL below.

The majority of the phase diagram (Fig. 1) consists of the magnetically ordered states familiar from the classical  $K$ - $J$ - $\Gamma$  model [11], namely AFM, stripe, incommensurate spiral (IS), zigzag, and FM ordered phases. Unsurprisingly, the boundaries around the QSL phases are rather different in the quantum model, with FM being stronger

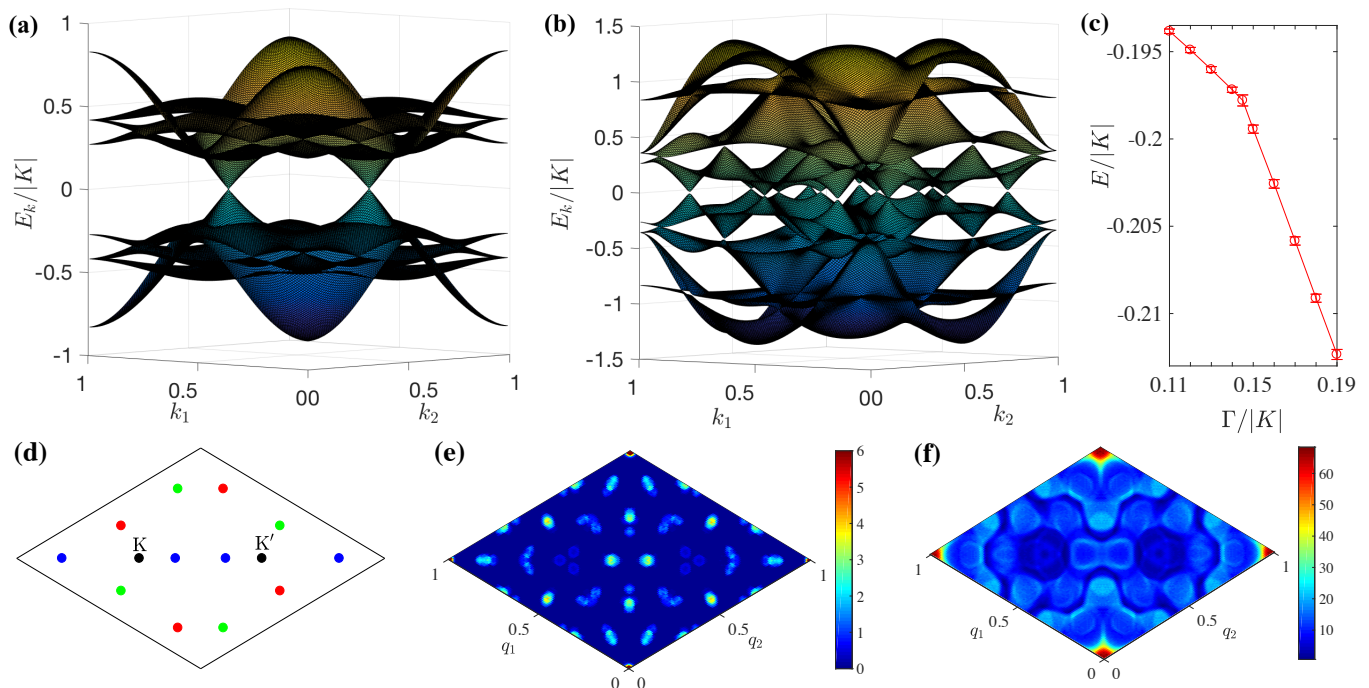


FIG. 2. (a) Spinon dispersion in the GKSL, drawn with  $\Gamma/|K| = 0.1$  and  $J = 0$ , showing 2 Majorana cones. (b) Spinon dispersion in the PKSL, drawn with  $\Gamma/|K| = 0.3$  and  $J = 0$ , showing 14 Majorana cones. (c) Ground-state energy per site of the  $K$ - $J$ - $\Gamma$  model at fixed  $J/|K| = 0.05$ , showing a clear first-order phase transition. (d) Locations of the 14 cones of the PKSL in the first Brillouin zone. (e) Dynamical structure factor of the PKSL at low energy (integrated over energies  $0 \leq \omega/|K| \leq 0.08$ ). (f) Dynamical structure factor of the PKSL at  $\omega/|K| = 0.15$  (integrated over  $0.13 \leq \omega/|K| \leq 0.17$ ).

at low  $\Gamma$  and IS extending to  $J < 0$ . We comment that, not only can an incommensurate ordered phase still exist for  $S = 1/2$ , but it can also exist throughout the phase diagram from (near) a pure  $K$ - $\Gamma$  to a pure  $J$ - $\Gamma$  model; as expected of our ordered phases, the spiral angles we obtain agree with Ref. [11]. We draw attention to the fact that all of the  $J = 0$  line in Fig. 1 is ordered for  $\Gamma/|K| > 0.55$ , with IS order until  $\Gamma/|K| = 0.7$  and zigzag order all the way to and in the pure  $\Gamma$  model [39]. This result contradicts an iDMRG study [25] that reported only QSL phases in the  $K$ - $\Gamma$  model; as we show in Sec. S4 of the SM [27], that conclusion is relevant only for very narrow cylinders. While the existence of order has been called into question at  $J = 0$  [21], it is robust in the  $S = 1/2$  model in VMC.

We state without demonstration that all of the phase transitions between the magnetically ordered phases are first-order, which is the simplest possibility when two phases of differing order parameters meet. A more complex situation is possible for the transitions between ordered and QSL phases, which could be second-order or even show an intermediate phase with coexisting magnetic and  $Z_2$  topological order (Sec. S3 of the SM [27]). However, we find at all points we have investigated that these transitions are also first-order. Finally, the transition between the GKSL and PKSL is also sharply first-order, as may be observed both in the ground-state en-

ergy [Fig. 2(c)] and through discontinuities in the optimal variational parameters (not shown). Neither the GKSL nor the PKSL dispersion [Figs. 2(a) and 2(b)] evolves significantly around the level-crossing.

Returning to the spin response of the QSLs, it is helpful to consider Kitaev's representation [1] of the spin in terms of Majorana fermions,  $S^m = ib^m c$  ( $m = x, y, z$ ), which we review in Sec. S1 of the SM [27]. In the GKSL, the  $c$  fermions are gapless and the  $b^m$  fermions gapped, but the gapped spin response of the KSL becomes gapless when both  $J$  and  $\Gamma$  are non-zero [36]. This is verified in our VMC calculations in the form of  $c$ - $b^m$  hybridization in the low-energy limit, but as shown in Sec. S5 of the SM [27] this hybridization remains very weak throughout the GKSL regime, such that low-energy spin excitations, if present, have very little weight. By contrast, in the PKSL we find that the quasiparticles are strongly hybridized combinations of  $c$  and  $b^m$  fermions at all wave vectors and energies, which is a consequence of the finite  $\eta_3$  parameter induced by the  $\Gamma$  term. Thus low-energy spin excitations arise from both intra- and intercone spinon processes and the spin response of the PKSL is gapless, as we illustrate in Fig. 2(e) by computing the dynamical structure factor,  $S(\mathbf{q}, \omega)$ , at the mean-field level for energy  $\omega = 0$  (Sec. S5). The positions of the maxima are readily understood from the cone structure shown in Fig. 2(d). For energies beyond the cone region,  $S(\mathbf{q}, \omega)$

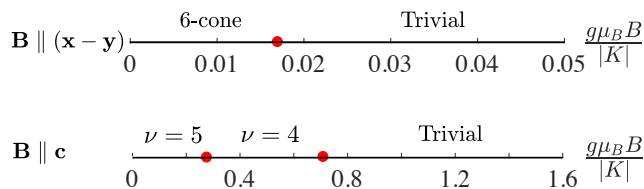


FIG. 3. Phase diagrams of the PKSL ( $\Gamma/|K| = 0.3$ ,  $J = 0$ ) in a magnetic field applied in the  $\hat{x} - \hat{y}$  direction and in the  $\hat{c} = \frac{1}{\sqrt{3}}(\hat{x} + \hat{y} + \hat{z})$  direction. “6-cone” denotes a phase whose low-energy spinon dispersion has six remaining cones.

takes on a complex and continuous form [Fig. 2(f)].

One of the most exciting properties of the KSL is that it becomes a gapped, non-Abelian CSL in an applied magnetic field of any orientation not orthogonal to an Ising (spin) axis. Specifically, Kitaev classified 16 different types of CSL based on the statistics of their vortices, which are defects arising from inserted flux quanta [1]. He showed that these  $Z_2$  vortices are Abelian anyons when the Chern number,  $\nu$ , is even and non-Abelian anyons when  $\nu$  is odd, leading to a clear illustration of topological properties, edge modes, fusion rules, and applications in quantum computation. The KSL in a field provides an example of the class  $\nu = 1$ , where the non-Abelian statistics arise due to unpaired Majorana modes ( $\sigma$  in Table I) associated with the vortices. By VMC calculations in a field  $\mathbf{B} \parallel \hat{c}$  (Sec. S6 of the SM [27]), we verify at the mean-field level that these modes are also present in the GKSL; this non-Abelian regime is terminated at a  $Z_2$  deconfinement-to-confinement transition [38].

In the PKSL, each of the 7 pairs of cones becomes gapped in a field  $\mathbf{B} \parallel \hat{c}$  and contributes a Chern number  $\nu = \pm 1$ . We demonstrate by VMC calculations at  $\Gamma/|K| = 0.3$  and  $J = 0$  that a CSL phase with  $\nu = 5$  is obtained at small  $|\mathbf{B}|$ . As shown in Fig. 3, there are two successive, weakly first-order phase transitions with increasing  $|\mathbf{B}|$ , to a  $\nu = 4$  CSL and then to a trivial phase connected to the fully polarized state. (We comment that this trivial,  $Z_2$ -confined phase is obtained from both the  $\nu = 1$  and  $\nu = 0$  mean-field states, as shown in Sec. S6 of the SM [27].) Thus the PKSL provides a specific realization of two little-known cases from Kitaev’s “16-fold way,” and we use it in Sec. S6 to illustrate their vortex modes at the mean-field level. The  $\nu = 5$  phase is a non-Abelian CSL while the  $\nu = 4$  phase is Abelian. Quite generally, in a CSL with Chern number  $\nu$ , there are  $\nu$  branches of chiral Majorana edge states, each of which contributes to a total chiral central charge  $c_- = \nu/2$ . The thermal Hall conductance, which is a physical observable, is therefore quantized to  $\kappa_{xy}/T\Lambda = c_-$ , where  $\Lambda = \pi k_B^2/6h$  is a constant. From the number of associated mid-gap modes it can be shown that the vortex carries topological spin  $e^{i\nu\frac{\pi}{8}}$ , and from its fusion with itself or with a fermion we obtain the anyonic character of the

Parent state	CSL	topological sectors	GSD	$c_-$
PKSL	$\nu = 5$	$\sigma, \varepsilon, 1$	3	5/2
PKSL	$\nu = 4$	$e, m, \varepsilon, 1$	4	2
KSL	$\nu = 1$	$\sigma, \varepsilon, 1$	3	1/2
U(1) Dirac	KL	$e, 1$	2	1

TABLE I. Field-induced CSL states realized to date in  $K$ - $J$ - $\Gamma$  models.  $\nu$  is the Chern number. KL is the Kalmayer-Laughlin state [23, 40]. 1 denotes the vacuum and  $\varepsilon$  the fermion.  $\sigma$  denotes the vortices in the non-Abelian phases ( $\nu = 1$  and 5), which have topological spin  $e^{i\frac{\pi}{8}}$  and  $e^{i\frac{5\pi}{8}}$ .  $e$  and  $m$  are the two different types of vortex in the Abelian CSL ( $\nu = 4$ ), which are both semions. GSD abbreviates the ground-state degeneracy on a torus.  $c_-$  is the chiral central charge.

CSLs as listed in Table I. These results are further verified within our VMC analysis by calculating the ground-state degeneracy (GSD) on a torus, which matches the number of topologically distinct quasiparticle types.

In contrast to the emergence in an arbitrary applied field of fully gapped quantum states, which can be distinguished by their  $\nu$  or edge  $c_-$  numbers, is the possibility that, for specific field directions, the system remains a gapless  $Z_2$  QSL over a finite range of field magnitudes [23]. In the PKSL we find this to be the case for  $\mathbf{B} \parallel (\mathbf{x} - \mathbf{y})$ , where the six black and blue cones shown in Fig. 2(d) remain gapless at low fields, whereas the other cones become gapped. For  $\mathbf{B} \parallel (\mathbf{y} - \mathbf{z})$ , the black and red cones remain gapless and for  $\mathbf{B} \parallel (\mathbf{z} - \mathbf{x})$  the black and green cones. With increasing field, pairs of cones move towards each other, but a first-order transition occurs to a fully gapped state at a critical field  $B_c \simeq 0.017|K|/g\mu_B$  (Fig. 3). This reflects the fact that many competing states appear at these low energy scales. We leave the response of the PKSL to fields of arbitrary orientation and strength to a future study.

The  $K$ - $J$ - $\Gamma$  model is expected to provide the basis for interpreting the physics of 4d and 5d transition-metal compounds. While robust magnetic order suggests strong  $J$  terms in  $\text{Li}_2\text{IrO}_3$  and  $\text{Na}_2\text{IrO}_3$  [4, 5],  $\alpha\text{-RuCl}_3$  is thought to have only weak  $J$  [20] and many different  $K$  and  $\Gamma$  combinations have been suggested [21, 22]. Our phase diagram provides a quantitative guide to the low- $J$ , low- $\Gamma$  parameter regime required to observe QSL behavior, including by application of pressure to the known candidate materials. It also offers a detailed framework within which to interpret both the physics of the magnetically disordered material  $\text{H}_3\text{LiIr}_2\text{O}_6$  [10] and the reported observation of a half-integer-quantized thermal Hall conductance in  $\alpha\text{-RuCl}_3$  [41].

In summary, we have obtained the phase diagram of the quantum  $K$ - $J$ - $\Gamma$  model on the honeycomb lattice. We find two quantum spin-liquid phases, the generic KSL and one proximate KSL, that have the same projective symmetry group but quite different low-energy physics. The PKSL is a gapless  $Z_2$  QSL with 14 Majorana cones

and a gapless spin response. In an applied field it realizes a gapped, non-Abelian chiral QSL with  $\nu = 5$  and an Abelian one with  $\nu = 4$ . We also map the wide variety of magnetically ordered phases appearing in the quantum limit. Our phase diagram provides an essential guide to the physics of candidate Kitaev materials.

*Acknowledgments.* We thank M. Cheng, H.-J. Liao, Q. Luo, M. Vojta, C. Wang, T. Xiang, Q. Wang, and especially Y.-M. Lu and L. Zou for helpful discussions. This work was supported by the Ministry of Science and Technology of China (Grant No. 2016YFA0300504), the NSF of China (Grant No. 11574392 and No. 11974421), and the Fundamental Research Funds for the Central Universities and the Research Funds of Renmin University of China (No. 19XNGL11).

---

\* [liuzxphys@ruc.edu.cn](mailto:liuzxphys@ruc.edu.cn)

- [1] A. Kitaev, *Ann. Phys.* **321**, 2 (2006).
- [2] G. Jackeli and G. Khaliullin, *Phys. Rev. Lett.* **102**, 017205 (2009).
- [3] J. Chaloupka, G. Jackeli, and G. Khaliullin, *Phys. Rev. Lett.* **105**, 027204 (2010).
- [4] F. Ye, S. X. Chi, H. B. Cao, B. C. Chakoumakos, J. A. Fernandez-Baca, R. Custelcean, T. F. Qi, O. B. Korneta, and G. Cao, *Phys. Rev. B* **85**, 180403(R) (2012).
- [5] S. K. Choi, R. Coldea, A. N. Kolmogorov, T. Lancaster, I. I. Mazin, S. J. Blundell, P. G. Radaelli, Y. Singh, P. Gegenwart, K. R. Choi, S.-W. Cheong, P. J. Baker, C. Stock, and J. Taylor, *Phys. Rev. Lett.* **108**, 127204 (2012).
- [6] J. M. Fletcher, W. E. Gardner, A. C. Fox, and G. Topping, *J. Chem. Soc. A* 1038 (1967).
- [7] J. A. Sears, M. Songvilay, K. W. Plumb, J. P. Clancy, Y. Qiu, Y. Zhao, D. Parshall, and Y.-J. Kim, *Phys. Rev. B* **91**, 144420 (2015).
- [8] R. D. Johnson, S. C. Williams, A. A. Haghighirad, J. Singleton, V. Zapf, P. Manuel, I. I. Mazin, Y. Li, H. O. Jeschke, R. Valentí, and R. Coldea, *Phys. Rev. B* **92**, 235119 (2015).
- [9] H. B. Cao, A. Banerjee, J.-Q. Yan, C. A. Bridges, M. D. Lumsden, D. G. Mandrus, D. A. Tennant, B. C. Chakoumakos, and S. E. Nagler, *Phys. Rev. B* **93**, 134423 (2016).
- [10] K. Kitagawa, T. Takayama, Y. Matsumoto, A. Kato, R. Takano, Y. Kishimoto, S. Bette, R. Dinnebier, G. Jackeli, and H. Takagi, *Nature* **554**, 341 (2018).
- [11] J. G. Rau, E.-H. Lee, and H.-Y. Kee, *Phys. Rev. Lett.* **112**, 077204 (2014).
- [12] I. A. Leahy, C. A. Pocs, P. E. Siegfried, D. Graf, S.-H. Do, K.-Y. Choi, B. Normand, and M. Lee, *Phys. Rev. Lett.* **118**, 187203 (2017).
- [13] S.-H. Baek, S.-H. Do, K.-Y. Choi, Y. S. Kwon, A. U. B. Wolter, S. Nishimoto, J. van den Brink, and B. Büchner, *Phys. Rev. Lett.* **119**, 037201 (2017).
- [14] J. Zheng, K. Ran, T. Li, J. Wang, P.-S. Wang, B. Liu, Z.-X. Liu, B. Normand, J. Wen, and W. Yu *Phys. Rev. Lett.* **119**, 227208 (2017).
- [15] A. Banerjee, P. Lampen-Kelley, J. Knolle, C. Balz, A. A. Aczel, B. Winn, Y. Liu, D. Pajerowski, J.-Q. Yan, C. A. Bridges, A. T. Savici, B. C. Chakoumakos, M. D. Lumsden, D. A. Tennant, R. Moessner, D. G. Mandrus, and S. E. Nagler, *npj Quantum Materials* **3**, 8 (2018).
- [16] Y. Cui, J. Zheng, K. Ran, J. Wen, Z.-X. Liu, B. Liu, W. Guo, and W. Yu, *Phys. Rev. B* **96**, 205147 (2017).
- [17] S. M. Winter, Y. Li, H. O. Jeschke, and R. Valentí, *Phys. Rev. B* **93**, 214431 (2016).
- [18] A. Banerjee, J. Q. Yan, J. Knolle, C. A. Bridges, M. B. Stone, M. D. Lumsden, D. G. Mandrus, D. A. Tennant, R. Moessner, and S. E. Nagler, *Science* **356**, 1055 (2017).
- [19] K. Ran, J. Wang, W. Wang, Z.-Y. Dong, X. Ren, S. Bao, S. Li, Z. Ma, Y. Gan, Y. Zhang, J. T. Park, G. Deng, S. Danilkin, S.-L. Yu, J.-X. Li, and J. Wen, *Phys. Rev. Lett.* **118**, 107203 (2017).
- [20] W. Wang, Z.-Y. Dong, S.-L. Yu, and J.-X. Li, *Phys. Rev. B* **96**, 115103 (2017).
- [21] L. Janssen, E. C. Andrade, and M. Vojta, *Phys. Rev. B* **96**, 064430 (2017).
- [22] J. Cookmeyer and J. E. Moore *Phys. Rev. B* **98**, 060412(R) (2018).
- [23] Z.-X. Liu and B. Normand, *Phys. Rev. Lett.* **120**, 187201 (2018).
- [24] A. Catuneanu, Y. Yamaji, G. Wachtel, Y.-B. Kim, and H.-Y. Kee, *npj Quantum Materials* **3**, 23 (2018).
- [25] M. Gohlke, G. Wachtel, Y. Yamaji, F. Pollmann, and Y. B. Kim, *Phys. Rev. B* **97**, 075126 (2018).
- [26] I. Affleck, Z. Zou, T. Hsu, and P. W. Anderson, *Phys. Rev. B* **38**, 745 (1988).
- [27] See the Supplemental Material at [url], for details concerning the fermionic spinon representation, IGG and PSG, finite-size effects, calculation of the dynamical structure factor, and field-induced topological states in the PKSL, which includes Ref. [28–34].
- [28] A. Kitaev, *AIP Conference Proceedings* **1134**, 22 (2009).
- [29] Xiao-Gang Wen, *Phys. Rev. B* **85**, 085103 (2012).
- [30] H.-H. Tu, *Phys. Rev. B* **87**, 041103(R) (2013).
- [31] S. Yang, T. B. Wahl, H.-H. Tu, N. Schuch, and J. I. Cirac, *Phys. Rev. Lett.* **114**, 106803 (2015).
- [32] M. Greiter and R. Thomale, *Phys. Rev. Lett.* **102**, 207203 (2009).
- [33] Z.-X. Liu, H.-H. Tu, Y.-H. Wu, R.-Q. He, X.-J. Liu, Y. Zhou, and T.-K. Ng, *Phys. Rev. B* **97**, 195158 (2018).
- [34] C. Nayak, S. H. Simon, A. Stern, M. Freedman, and S. Das Sarma, *Rev. Mod. Phys.* **80**, 1083 (2008).
- [35] X.-G. Wen, *Phys. Rev. B* **65**, 165113 (2002).
- [36] X.-Y. Song, Y.-Z. You, and L. Balents, *Phys. Rev. Lett.* **117**, 037209 (2016).
- [37] Y.-Z. You, I. Kimchi, and A. Vishwanath, *Phys. Rev. B* **86**, 085145 (2012).
- [38] H.-C. Jiang, Z.-C. Gu, X.-L. Qi, and S. Trebst, *Phys. Rev. B* **83**, 245104 (2011).
- [39] H. J. Liao, R. Z. Huang, Y. B. Guo, Z. Y. Xie, B. Normand, and T. Xiang, unpublished.
- [40] V. Kalmeyer and R. B. Laughlin, *Phys. Rev. Lett.* **59**, 2095 (1987).
- [41] Y. Kasahara, T. Ohnishi, Y. Mizukami, O. Tanaka, S. Ma, K. Sugii, N. Kurita, H. Tanaka, J. Nasu, Y. Motome, T. Shibauchi, and Y. Matsuda, *Nature* **559**, 227 (2018).

# Supplemental Material for “One Proximate Kitaev Spin Liquid in the $K$ - $J$ - $\Gamma$ Model on the Honeycomb Lattice”

Jiucui Wang, B. Normand, and Zheng-Xin Liu

## S1. FERMIONIC SPINON REPRESENTATION

### A. SU(2) gauge structure

A detailed introduction to the fermionic spin representation, by which the spinons  $C = (c_\uparrow, c_\downarrow)^T$  are used to express the spin operators as  $S^m = \frac{1}{2}C^\dagger \sigma^m C$ , may be found in Sec. S1 of Ref. [1]. The two spinon species may further be expressed in terms of four Majorana fermions,

$$c_\uparrow = \frac{1}{2}(b^z + ic), \quad c_\downarrow = \frac{1}{2}(b^x + ib^y), \quad (\text{S1})$$

which satisfy the anti-commutation relations  $\{b^\alpha, b^\beta\} = 2\delta^{\alpha\beta}$  ( $\alpha, \beta = 0, x, y, z$ ;  $b^0 \equiv c$ ). In this basis, the spin operator takes the form

$$S^m = ib^m c, \quad (\text{S2})$$

and the particle-number constraint,  $C^\dagger C = 1$ , is  $b^x b^y b^z c = 1$ .

The anti-commutation relation of the Majorana fermions is invariant under the group SO(4). The relation  $\text{SO}(4) \simeq \text{SU}(2) \times \text{SU}(2) / \mathbb{Z}_2$  expresses the fact that the Majorana fermions are invariant under two types of SU(2) operation, one being the expected spin-rotation group and the other a “particle-hole-type” charge rotation, which behaves as an internal gauge symmetry for the fermionic representation of spin  $S = 1/2$ .

It is convenient to introduce the time-reversal and particle-hole partner of  $C$ , namely  $\bar{C} = (c_\downarrow^\dagger, -c_\uparrow^\dagger)^T$ , in terms of which the spin operator may also be expressed as  $S^m = \frac{1}{2}\bar{C}^\dagger \sigma^m C$ .  $C$  and  $\bar{C}$  can be combined into a matrix operator,

$$\psi = (C \ \bar{C}) = \begin{pmatrix} c_\uparrow & c_\downarrow^\dagger \\ c_\downarrow & -c_\uparrow^\dagger \end{pmatrix} = \frac{1}{2}(ic + b^x \tau_x + b^y \tau_y + b^z \tau_z),$$

to obtain a symmetric representation of the spin operators as  $S^m = \frac{1}{4}\text{Tr}(\psi^\dagger \sigma^m \psi)$ , while the particle-number constraint is  $\text{Tr}(\psi \tau^z \psi^\dagger) = 0$ , where we use the Pauli matrix  $\tau^z$  to distinguish from the spin operation  $\sigma^z$ .

In this framework, a left SU(2) transformation,  $\psi \rightarrow g^\dagger \psi$  (or equivalently  $\psi^\dagger \rightarrow \psi^\dagger g$ ), mixes  $c_\uparrow$  and  $c_\downarrow$  and thus corresponds to a spin rotation,

$$\frac{1}{4}\text{Tr}(\psi^\dagger g \sigma^m g^\dagger \psi) = \sum_n R_{nm}(g) S^n,$$

where  $R(g)$  is an SO(3) matrix representation of  $g$ . By contrast, a right SU(2) transformation,  $\psi \rightarrow \psi W$ , mixes  $C$  and  $\bar{C}$  and corresponds to the SU(2) gauge symmetry,

$$\frac{1}{4}\text{Tr}(W^\dagger \psi \tau^m \psi^\dagger W) = \sum_n R(W)_{nm} \Lambda^n,$$

where  $\Lambda^m = \frac{1}{4}\text{Tr}(\psi \tau^m \psi^\dagger)$  are the generators of the SU(2) gauge transformation in the same way that the spin operators  $S^m = \frac{1}{4}\text{Tr}(\psi^\dagger \sigma^m \psi)$  are the generators of the SU(2) spin rotation. It is easy to see that  $\mathbf{\Lambda}$  is spin-rotation-invariant and  $\mathbf{S}$  is SU(2) gauge-invariant. In this notation, the particle-number constraint ( $\text{Tr}(\psi \tau^z \psi^\dagger) = 0$ ) can be written in the SU(2) gauge-covariant form  $\mathbf{\Lambda} = 0$ , i.e.

$$\text{Tr}(\psi \boldsymbol{\tau} \psi^\dagger) = 0, \quad (\text{S3})$$

which specifies that the physical Hilbert space is SU(2) gauge-invariant.

### B. Mean-field Hamiltonian

The Heisenberg exchange interaction can be written as

$$\begin{aligned} \mathbf{S}_i \cdot \mathbf{S}_j &= -\frac{1}{8}\text{Tr}(\psi_j^\dagger \psi_i \psi_i^\dagger \psi_j) \\ &= \frac{1}{8}\text{Tr}(\psi_j^\dagger \boldsymbol{\sigma} \psi_i \cdot \psi_i^\dagger \boldsymbol{\sigma} \psi_j) \end{aligned} \quad (\text{S4})$$

up to constant terms. To make more transparent the connection to the spinon representation, we note that the singlet matrix operator,  $\psi_i^\dagger \psi_j$ , and the triplet operator,  $\psi_i^\dagger \boldsymbol{\sigma} \psi_j$ , can be expanded as

$$\psi_i^\dagger \psi_j = \begin{pmatrix} C_i^\dagger C_j & C_i^\dagger \bar{C}_j \\ \bar{C}_i^\dagger C_j & \bar{C}_i^\dagger \bar{C}_j \end{pmatrix}, \quad \psi_i^\dagger \boldsymbol{\sigma} \psi_j = \begin{pmatrix} C_i^\dagger \boldsymbol{\sigma} C_j & C_i^\dagger \boldsymbol{\sigma} \bar{C}_j \\ \bar{C}_i^\dagger \boldsymbol{\sigma} C_j & \bar{C}_i^\dagger \boldsymbol{\sigma} \bar{C}_j \end{pmatrix}.$$

The sign difference between the two decoupling formulas in Eq. (S4) means that the version in the first line is suitable for AFM Heisenberg interactions and that in the second line for FM ones.

In the mean-field approximation, one decouples these interactions to obtain a non-interacting fermionic Hamiltonian. In the AFM case ( $J > 0$ )

$$H_{\text{mf}} = -J \sum_{\langle i, j \rangle} \text{Tr}(U_{ij}^\dagger \psi_i^\dagger \psi_j + \text{h.c.}) + \sum_i \boldsymbol{\lambda} \cdot \mathbf{\Lambda}_i, \quad (\text{S5})$$

while in the FM one ( $J < 0$ )

$$H_{\text{mf}} = J \sum_{\langle i, j \rangle} \text{Tr}(U_{ij}^\dagger \psi_i^\dagger \boldsymbol{\sigma} \psi_j + \text{h.c.}) + \sum_i \boldsymbol{\lambda} \cdot \mathbf{\Lambda}_i, \quad (\text{S6})$$

where  $\boldsymbol{\lambda}$  are the Lagrange multipliers corresponding to Eq. (S3),  $U_{ij}^\dagger = U_{ji} \propto \langle \psi_j^\dagger \psi_i \rangle$  is a matrix of singlet parameters and  $\mathbf{U}_{ij}^\dagger = \mathbf{U}_{ji} \propto \langle \psi_j^\dagger \boldsymbol{\sigma} \psi_i \rangle$  is a triplet parameter matrix. Under the gauge transformation  $\psi_i \rightarrow \psi_i W_i$ ,

$$\begin{aligned} \text{Tr}(U_{ij}^\dagger \psi_i^\dagger \psi_j) &\rightarrow \text{Tr}(U_{ij}^\dagger W_i^\dagger \psi_i^\dagger \psi_j W_j) \\ &= \text{Tr}(W_j U_{ij}^\dagger W_i^\dagger \psi_i^\dagger \psi_j), \end{aligned} \quad (\text{S7})$$

meaning that  $U_{ji} \rightarrow U'_{ji} = W_j U_{ji} W_i^\dagger$  varies as an SU(2) gauge field and similarly for  $\mathbf{U}_{ji} \rightarrow \mathbf{U}'_{ji} = W_j \mathbf{U}_{ji} W_i^\dagger$ . Thus the spin system is described in the mean-field theory by free fermions coupling to static SU(2) gauge fields on the bonds of the honeycomb lattice.

In insulating systems with spin-orbit coupling, the spin interactions are anisotropic, as expressed in the  $K$ - $J$ - $\Gamma$  Hamiltonian [Eq. (1) of the main text]. In this case the mean-field Hamiltonian will contain both singlet ( $\psi_i^\dagger \psi_j$ ) and triplet terms ( $\psi_i^\dagger \boldsymbol{\sigma} \psi_j$ ). As an example, an AFM Ising interaction can be decoupled [1] as

$$S_i^m S_j^m = -\frac{1}{16} \left[ \text{Tr}(\psi_i^\dagger \psi_j \psi_j^\dagger \psi_i) + \text{Tr}(\psi_i^\dagger \boldsymbol{\sigma}^m \psi_j \psi_j^\dagger \boldsymbol{\sigma}^m \psi_i) \right],$$

up to a constant term, where  $m = x, y, z$ , and thus any XXZ-type interaction may be expressed by adding triplet hopping and pairing terms of the form  $\sum_{\langle i, j \rangle} \text{Tr}(U_{ij}^z \psi_i^\dagger \sigma^z \psi_j)$  to the mean-field Hamiltonian of Eq. (S5). The most general mean-field Hamiltonian for a spin-liquid state in a spin-orbit-coupled magnetic insulator, containing both (S5) and (S6), takes the form

$$H_{\text{mf}}^{\text{SL}} = \sum_{\langle i, j \rangle} \text{Tr}(U_{ji} \psi_i^\dagger \psi_j + \mathbf{U}_{ji} \cdot \psi_i^\dagger \boldsymbol{\sigma} \psi_j + \text{h.c.}) + \sum_i \boldsymbol{\lambda} \cdot \boldsymbol{\Lambda}_i, \quad (\text{S8})$$

where  $U_{ji}$  and  $\mathbf{U}_{ji}$  are treated as variational parameters.

## S2. INVARIANT GAUGE GROUP AND PROJECTIVE SYMMETRY GROUP

Because of the static bond gauge fields contained in  $U_{ji}$  and  $\mathbf{U}_{ji}$ , the mean-field Hamiltonian of Eq. (S8) is not in general invariant under an arbitrary SU(2) gauge transformation. The subgroup of the SU(2) gauge group under which Eq. (S8) remains invariant is called the invariant gauge group (IGG) of the spin-liquid state. The IGG determines the nature of the low-energy gauge fluctuations in a QSL phase.

If the IGG is U(1), there exists an SU(2) gauge transformation that eliminates all fermion-pairing terms in the mean-field Hamiltonian, meaning that the number of fermionic slave particles is conserved. In this case, the gapless gauge photons contribute to the low-energy excitations. In two spatial dimensions (2D), it is known that a U(1) gauge field is confined unless it is coupled to a matter field (in this case the fermions) that is either (i) gapless or (ii) has a nonzero Chern number.

If the IGG is  $Z_2$ , as in the KSL, fermion-pairing terms cannot be removed by any SU(2) gauge transformation. The  $Z_2$  gauge-flux excitations in this case are usually gapped, and can remain deconfined even if the matter field is gapped with zero Chern number. The low-energy gauge fluctuations dictated by the confinement or deconfinement of the  $Z_2$  gauge field are reflected in the ground-state degeneracy (GSD) of the QSL when placed on a torus: in the thermodynamic limit, inserting a global  $Z_2$

$\pi$  flux in either hole of the torus costs no energy. Because this process is equivalent to exchanging the boundary conditions of the mean-field Hamiltonian from periodic to anti-periodic, in 2D one may construct the four mean-field ground states  $|\psi_{\pm\pm}\rangle$ , where the subscripts denote the boundary conditions for the  $x$ - and  $y$ -directions. After a Gutzwiller projection of these four states to the physical Hilbert space, the number of linearly independent states is equal to the GSD on a torus.

We calculate the density matrix of the projected (VMC) states from the wave-function overlap  $\rho_{\alpha\beta} = \langle P_G \psi_\alpha | P_G \psi_\beta \rangle = \rho_{\beta\alpha}^*$ , with  $\alpha, \beta \in \{++, +-, -+, --\}$ . If  $\rho_{\alpha\beta}$  has only one significant eigenvalue, with the others vanishing, then the GSD is 1, indicating that the  $Z_2$  gauge field is confined. If  $\rho_{\alpha\beta}$  has more than one near-degenerate nonzero eigenvalue, the GSD is nontrivial and hence the  $Z_2$  gauge fluctuations are deconfined. In this deconfined phase, if the Chern number is even then from above the GSD is 4; however, if the Chern number is odd, as we will find in Sec. S6, then the GSD is 3 because the mean-field ground state  $|\psi_{++}\rangle$  has odd fermionic parity and vanishes after Gutzwiller projection.

Quite generally, a QSL should respect all the symmetries of the spin Hamiltonian, but at the mean-field level this constraint can be relaxed in the following sense. Under a symmetry operation  $g$ ,  $H_{\text{mf}}$  may be transformed to a different expression,  $gH_{\text{mf}} = H'_{\text{mf}} \neq H_{\text{mf}}$ , but if it can be transformed back to its original form by an SU(2) gauge transformation then this mean-field Hamiltonian still describes a spin-liquid state. Specifically,

$$\psi_i \rightarrow g^\dagger \psi_{g(i)} W_i(g), \quad (\text{S9})$$

$$\begin{aligned} \text{Tr}[\mathbf{U}_{ji} \cdot \psi_i^\dagger \boldsymbol{\sigma} \psi_j] &\rightarrow \text{Tr}[W_j \mathbf{U}_{ji} W_i^\dagger \cdot \psi_{g(i)}^\dagger g \boldsymbol{\sigma} g^\dagger \psi_{g(j)}] \\ &= \text{Tr}[\mathbf{U}_{g(j)g(i)} \cdot \psi_{g(i)}^\dagger \boldsymbol{\sigma} \psi_{g(j)}], \end{aligned} \quad (\text{S10})$$

$$\begin{aligned} \text{Tr}[U_{ji} \psi_i^\dagger \psi_j] &\rightarrow \text{Tr}[W_j U_{ji} W_i^\dagger \psi_{g(i)}^\dagger g g^\dagger \psi_{g(j)}] \\ &= \text{Tr}[U_{g(j)g(i)} \psi_{g(i)}^\dagger \psi_{g(j)}], \end{aligned} \quad (\text{S11})$$

which requires  $U_{g(j)g(i)}^n = \sum_m R_{nm}(g) W_j(g) U_{ji}^m W_i^\dagger(g)$  and  $U_{g(j)g(i)} = W_j(g) U_{ji} W_i^\dagger(g)$ . The new symmetry operations, each of which involves a symmetry operation  $g$  followed by a gauge transformation  $W_i(g)$ , form a larger group that is known as the projective symmetry group (PSG). Together with the IGG, the PSG of the mean-field Hamiltonian is used to classify and distinguish the different spin-liquid phases.

The gapless KSL is believed [2] to be a finite, stable phase in the presence of non-Kitaev interactions, including the  $J$  and  $\Gamma$  terms. The mean-field Hamiltonian describing the generic state around the KSL, which we denote the gKSL, will then respect the same PSG as the KSL itself. Besides translation symmetry, the symmetry group of the pure KSL,  $G = D_{3d} \times Z_2^T$ , has the three generators

$$S_6 = (C_3)^2 P, \quad M = C_2^{x-y} P, \quad T = i\sigma^y K,$$

where  $C_3$  is a threefold rotation around the direction  $\hat{c} =$

$\frac{1}{\sqrt{3}}(\hat{x}+\hat{y}+\hat{z})$ ,  $C_2^{x-y}$  is a twofold rotation around  $\frac{1}{\sqrt{2}}(\hat{x}-\hat{y})$ , and  $P$  is spatial inversion. The PSG of the KSL is read most simply from the Majorana representation, in which the mean-field Hamiltonian is

$$\begin{aligned} H_{\text{mf}}^K &= \sum_{\langle i,j \rangle \in \gamma} \rho_a (i c_i c_j) + \rho_c (i b_i^\gamma b_j^\gamma) \\ &= \sum_{\langle i,j \rangle \in \gamma} i \rho_a \text{Tr}(\psi_i^\dagger \psi_j + \tau^x \psi_i^\dagger \sigma^x \psi_j + \tau^y \psi_i^\dagger \sigma^y \psi_j \\ &\quad + \tau^z \psi_i^\dagger \sigma^z \psi_j) + i \rho_c \text{Tr}(\psi_i^\dagger \psi_j + \tau^\gamma \psi_i^\dagger \sigma^\gamma \psi_j \\ &\quad - \tau^\alpha \psi_i^\dagger \sigma^\alpha \psi_j - \tau^\beta \psi_i^\dagger \sigma^\beta \psi_j) + \text{h.c.} \end{aligned} \quad (\text{S12})$$

Because the  $c$  fermion never mixes with any of the  $b^m$  fermions, any PSG operation leaves the  $c$  fermions invariant. The gauge operation,  $W_i(g)$ , following the symmetry operation  $g$  should then be  $W_i(g) = \pm g$ . A detailed analysis [3] shows that the gauge transformations of the generators  $S_6$ ,  $M$ , and  $T$  are

$$\begin{aligned} W_A(S_6) &= -W_B(S_6) = \exp\left[-i\frac{4}{3}\pi\frac{1}{2\sqrt{3}}(\tau^x + \tau^y + \tau^z)\right], \\ W_A(M) &= -W_B(M) = \exp\left[-i\pi\frac{1}{2\sqrt{2}}(\tau^x - \tau^y)\right], \\ W_A(T) &= -W_B(T) = i\tau^y, \end{aligned} \quad (\text{S13})$$

where A and B denote the two sublattices of the honeycomb lattice.

### S3. $K$ - $J$ - $\Gamma$ MODEL: SYMMETRY-PROTECTION AND MAGNETIC ORDER

When the Kitaev model is extended to the  $K$ - $J$ - $\Gamma$  model, still with only nearest-neighbor coupling on the honeycomb lattice for all three types of term, there are several different ansatzes for states beyond the Kitaev mean-field Hamiltonian [Eq. (S12)] that are invariant under the same PSG. The  $\Gamma$  interaction gives rise to the mean-field terms

$$\begin{aligned} H_{\text{mf}}^\Gamma &= \sum_{\langle i,j \rangle \in \gamma} i \rho_d (b_i^\alpha b_j^\beta + b_i^\beta b_j^\alpha) \\ &= \sum_{\langle i,j \rangle \in \gamma} i \rho_d \text{Tr}\left(\tau^\alpha \psi_i^\dagger \sigma^\beta \psi_j + \tau^\beta \psi_i^\dagger \sigma^\alpha \psi_j\right) + \text{h.c.} \end{aligned} \quad (\text{S14})$$

It is readily demonstrated from the Majorana decoupling that Heisenberg interactions do not give rise to any new types of term. Thus when expressed in terms of  $U_{ij}$  and  $\mathbf{U}_{ij}$ , the full expression of the mean-field Hamiltonian that preserves the PSG is

$$\begin{aligned} H_{\text{mf}}^{\text{SL}} &= \sum_{\langle i,j \rangle \in \gamma} \text{Tr}[U_{ji}^{(0)} \psi_i^\dagger \psi_j] + \text{Tr}[U_{ji}^{(1)} \psi_i^\dagger (i R_{\alpha\beta}^\gamma) \psi_j] \\ &\quad + \text{Tr}[U_{ji}^{(2)} \psi_i^\dagger \sigma^\gamma \psi_j] + \text{Tr}[U_{ji}^{(3)} \psi_i^\dagger \sigma^\gamma R_{\alpha\beta}^\gamma \psi_j] + \text{h.c.}, \end{aligned} \quad (\text{S15})$$

where  $R_{\alpha\beta}^\gamma = -\frac{i}{\sqrt{2}}(\sigma^\alpha + \sigma^\beta)$ , which is Eq. (2) of the main text. The decouplings expressed in Eqs. (S12) and (S14)

contribute the terms

$$\begin{aligned} \tilde{U}_{ji}^{(0)} &= i(\rho_a + \rho_c), \\ \tilde{U}_{ji}^{(1)} &= i(\rho_a - \rho_c + \rho_d)(\tau^\alpha + \tau^\beta), \\ \tilde{U}_{ji}^{(2)} &= i(\rho_a + \rho_c)\tau^\gamma, \\ \tilde{U}_{ji}^{(3)} &= i(\rho_c - \rho_a - \rho_d)(\tau^\alpha - \tau^\beta), \end{aligned} \quad (\text{S16})$$

to the coefficients  $U_{ji}^{(m)}$ , in which  $j$  and  $i$  specify  $\gamma$ . However, the most general coefficients preserving the  $C_3$  rotation symmetry (in the PSG sense) also contain multiples of the uniform ( $I$ ) and  $\tau^x + \tau^y + \tau^z$  gauge components,

$$\begin{aligned} \tilde{\tilde{U}}_{ji}^{(0)} &= i\eta_0 + \eta_1(\tau^x + \tau^y + \tau^z), \\ \tilde{\tilde{U}}_{ji}^{(1)} &= \eta_2 + i\eta_3(\tau^x + \tau^y + \tau^z), \\ \tilde{\tilde{U}}_{ji}^{(2)} &= \eta_4 + i\eta_5(\tau^x + \tau^y + \tau^z), \\ \tilde{\tilde{U}}_{ji}^{(3)} &= \eta_6 + i\eta_7(\tau^x + \tau^y + \tau^z). \end{aligned} \quad (\text{S17})$$

If the full symmetry group,  $G = D_{3d} \times Z_2^T$ , is preserved, then only the three parameters  $\eta_0$ ,  $\eta_3$ , and  $\eta_5$  are allowed; by contrast, if one allows the breaking of spatial inversion symmetry, while still preserving mirror reflection symmetry, then  $\eta_1$ ,  $\eta_2$ , and  $\eta_4$  are also allowed. Thus a spin-liquid ansatz that preserves the full PSG symmetry generated by Eq. (S13) contains the variables  $U_{ji}^{(m)} = \tilde{U}_{ji}^{(m)} + \tilde{\tilde{U}}_{ji}^{(m)}$  of the main text with six real scalar parameters,  $\rho_a$ ,  $\rho_c$ ,  $\rho_d$ ,  $\eta_0$ ,  $\eta_3$ , and  $\eta_5$ . Of these, only  $\eta_3$  and  $\eta_5$  lead to a hybridization of the  $c$  with the  $b^m$  fermions, which as we show in Sec. S5 has important consequences for the spin response of the ground state.

#### A. Majorana Cones and Symmetry Protection

The  $G = D_{3d} \times Z_2^T$  symmetry imposes a constraint on the number of cones in the mean-field dispersion. First, the momentum points  $\mathbf{K}$  and  $\mathbf{K}'$  are invariant under the subgroup  $C_{3v}$ , together with the combined symmetry operation  $PT$ , and are transformed into each other either by time reversal ( $T$ ) or by spatial inversion ( $P$ ). The cones at  $\mathbf{K}$  and  $\mathbf{K}'$  must therefore appear as a pair. Second, if an extra cone appears at a general point  $\mathbf{k}$ , which in the present case must be invariant under one of the mirror-reflection operations in  $D_{3d}$ , then the  $C_3$  and  $C_3^2$  operations transform  $\mathbf{k}$  into  $\mathbf{k}'$  and  $\mathbf{k}''$ , respectively, while the time-reversal symmetry further transforms these three points into  $-\mathbf{k}$ ,  $-\mathbf{k}'$ ,  $-\mathbf{k}''$ . Because the spin liquid preserves the  $G = D_{3d} \times Z_2^T$  symmetry, cones should appear at all six of these points, and the total number of cones should be  $N = 2 + 6m$ , where  $m \geq 0$  is an integer.

Next we discuss the symmetry protecting these cones and hence guaranteeing their existence. It is known that the Berry phase along a small contour surrounding a cone is quantized to  $\pi$  and hence is nontrivial. However, without symmetry-protection, the cone can become gapped



and the corresponding Berry phase can be changed continuously. The key symmetry in the present case is the fact that the position of the cone is invariant under the combination  $PT$ : for any system with  $PT$  symmetry, the 1D subsystem defined by the contour also has this symmetry. From classification theory [4, 5], a gapped 1D fermionic system preserving this combined symmetry, with  $(PT)^2 = 1$ , is classified by  $Z_2$ , indicating that there is one nontrivial phase. Thus the  $\pi$ -quantization of the Berry phase along such a contour is  $PT$ -protected, and hence the stability of the cone is also protected. The  $Z_2$  classification also indicates that one mechanism for gapping of the cones in a system preserving  $PT$  symmetry is when two cones merge.

Besides being used to construct the mean-field ansatz, the PSG can also be used to classify QSL phases that have the same pattern of many-body entanglement but different types of symmetry fractionalization. However, the gKSL and PKSL phases of the present work have the same PSG but different patterns of many-body entanglement, and hence quite different physical properties. This difference becomes clear when a magnetic field is applied in the  $\hat{z}$ -direction, and the resulting gapped chiral spin-liquid (CSL) phases have different types of topological order, as we discuss in Sec. S6.

## B. Magnetic Order

In addition to spin-liquid phases, to describe the magnetic order of the spin-symmetry-breaking phases of the  $K$ - $J$ - $\Gamma$  model we introduce a single- $\mathbf{Q}$  field [6]

$$\mathbf{M}_i = M\{\sin\phi[\hat{\mathbf{e}}'_x \cos(\mathbf{Q} \cdot \mathbf{r}_i) + \hat{\mathbf{e}}'_y \sin(\mathbf{Q} \cdot \mathbf{r}_i)] + \cos\phi \hat{\mathbf{e}}'_z\},$$

where the local spin axes,  $\hat{\mathbf{e}}'_\alpha$ , are specified at  $\mathbf{r}_i = 0$  by three Euler angles,  $(\psi, \theta, \varphi)$ , and  $\phi$  is a canting angle. We determine  $(\psi, \theta, \varphi)$  from the classical ground state. Although  $\phi$  is treated as a variational parameter, we find in all our ordered ground states except for the IS phase that the canting angle  $\phi \rightarrow 0$ . Thus the quantum corrections we compute are in essence contained in the amplitude of the ordered moment,  $M$ . In this way, the static order is treated as an external field, obtained by summing over all neighbors of a given site,  $i$ , and hence the full mean-field Hamiltonian for the  $K$ - $J$ - $\Gamma$  model is

$$H_{\text{mf}}^{\text{total}} = H_{\text{mf}}^{\text{SL}} - \frac{1}{2} \sum_i (\mathbf{M}_i \cdot C_i^\dagger \boldsymbol{\sigma} C_i + \text{h.c.}). \quad (\text{S18})$$

The ground state of  $H_{\text{mf}}^{\text{total}}$  preserves all of the symmetries of the PSG or the ordered magnetic state. The trial wave functions obtained by Gutzwiller projection then also preserve the full symmetry of the system.

In order to provide a complete and systematic study of the  $K$ - $J$ - $\Gamma$  phase diagram, we have investigated many different ansatzes for both the spin-liquid and the ordered magnetic phases. In the spin-liquid regime of Fig. 1 of the main text, one of the most important questions [1] is

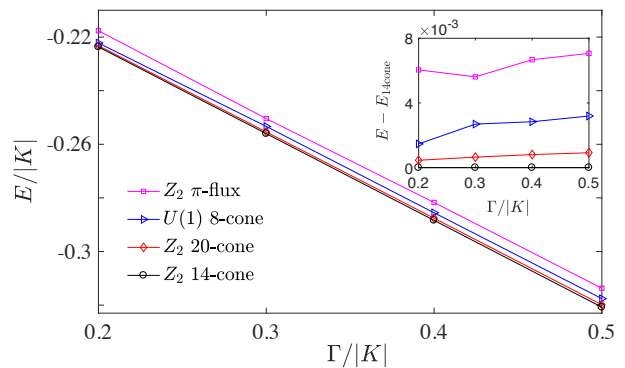


FIG. S1. Ground-state energy per site,  $E$ , of the  $K$ - $\Gamma$  model ( $J = 0$ ), comparing the lowest-lying trial wave functions for  $U(1)$  and  $Z_2$  QSLs. The inset shows the energy difference from the 14-cone  $Z_2$  state.

whether states with IGG  $U(1)$  can compete with states whose IGG is  $Z_2$  (but whose PSG may be different from that of the KSL). As Fig. S1 illustrates for the  $J = 0$  line, in the absence of an applied field even the leading (8-cone)  $U(1)$  state is not favored energetically in the parameter range of the PKSL.

Turning to  $Z_2$  QSLs, we have found a 20-cone state that lies very low in energy and has the same PSG as the 14-cone state. As a technical comment, we count the number of cones in any state by using the parameters determined from VMC to draw the spinon dispersion of Eq. (S15) in a momentum space of  $120 \times 120$   $\mathbf{k}$ -points. Physically, although we will show in Sec. S4 that the 20-cone state is not favored energetically for any large system sizes, it is instructive to present a brief discussion of its properties. In the 20-cone state, the  $b_x$ ,  $b_y$ , and  $b_z$  fermions are mutually hybridized, but in contrast to the 14-cone state they have almost no hybridization with the  $c$  fermions. This is a consequence of the variational parameters  $\eta_3$  and  $\eta_5$  being finite in the 14-cone state but very small in the 20-cone state. Further, a weak out-of-plane field applied to the 20-cone state induces an Abelian CSL with Chern number  $\nu = 4$ , rather than the non-Abelian CSL with  $\nu = 5$  induced from the 14-cone phase (main text). Another candidate QSL is the  $\pi$ -flux state, which contains a  $\pi$ -flux in every hexagon and thus has a different PSG. In summary, although the 14-cone state is the ground state over the full PKSL regime, it is clear from Fig. S1 that indeed there exist several competing states which are very close in energy, despite their quite different physical nature.

We also tested many different ansatzes for the ordered magnetic states. Here we found without exception that ordered states with IGG  $Z_2$  in  $H_{\text{mf}}^{\text{SL}}$  are favored. Because the gauge-flux excitations (visons) are gapped in a  $Z_2$  QSL, they may remain deconfined even in the presence of magnetic order. Alternatively stated, a phase with coexisting magnetic order and  $Z_2$  topological order is allowed in principle, and would be separated both from the nearest pure spin-liquid phase and from the pure magnet-

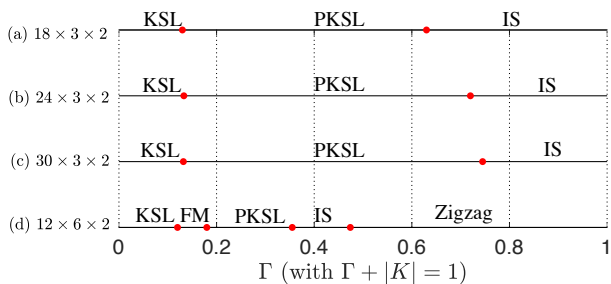


FIG. S2. Phase diagram of the  $K$ - $\Gamma$  model ( $K < 0$ ) in a cylindrical geometry, shown on a scale where  $|K| + \Gamma = 1$ . (a)-(c) Cylinders of radius 6 sites: QSL phases dominate, their regime of stability increasing with cylinder length. (d) System size  $12 \times 6 \times 2$ : three magnetically ordered phases appear. The variational parameters of the QSL phases we denote by PKSL in panels (a)-(c) correspond in a 2D system to the 14-cone state, but in panel (d) to the 20-cone state.

ically ordered phase by continuous transitions. However, our VMC results indicate that such coexisting states do not appear in the phase diagram: all of the magnetically ordered ground states we find have singly degenerate ground states on a torus, indicating the absence of  $Z_2$  topological order. Thus it is no surprise that all the transitions from spin-liquid to magnetically ordered phases in Fig. 1 of the main text are first-order.

Similar conditions are found in the presence of an applied magnetic field (Sec. S6). Because the IGG is  $Z_2$ , when all the cones are gapped by the magnetic field and the total Chern number vanishes, it remains possible that the system can possess  $Z_2$  topological order. However, such states never appear in the VMC phase diagram, i.e. gapped states in the  $K$ - $J$ - $\Gamma$  model with zero Chern number are always  $Z_2$ -confined and trivial.

#### S4. FINITE-SIZE EFFECTS IN THE $K$ - $\Gamma$ MODEL

As stated in the main text, the phase boundaries we find by VMC for the  $K$ - $J$  model, meaning the model with  $\Gamma = 0$  and  $J > 0$ , agree quantitatively with the results obtained by DMRG [13]. Specifically, we find that  $J_{c1} = 0.16|K|$  for the transition from the KSL into the spiral phase and  $J_{c2} = 0.77|K|$  for the AFM transition, while in Ref. [13]  $J_{c1} = 0.13|K|$  and  $J_{c2} = 0.75|K|$ . This indicates that finite-size effects in the  $K$ - $J$  model, which in DMRG arise from the circumference of the cylinder used, are relatively weak.

However, the situation is different for the  $K$ - $\Gamma$  model. In Ref. [7] it was stated that the ground state of the  $K$ - $\Gamma$  model with  $K < 0$  and  $\Gamma > 0$  is magnetically disordered for all values of  $\Gamma/|K|$ , a result quite different from our conclusion (Fig. 1 of the main text). We note that the iDMRG calculations of these authors were performed on cylinders with a circumference of six lattice sites. To reproduce this geometry, we perform VMC calculations for the model with  $J = 0$  on lattices of sizes  $L_x \times L_y \times 2$ ,

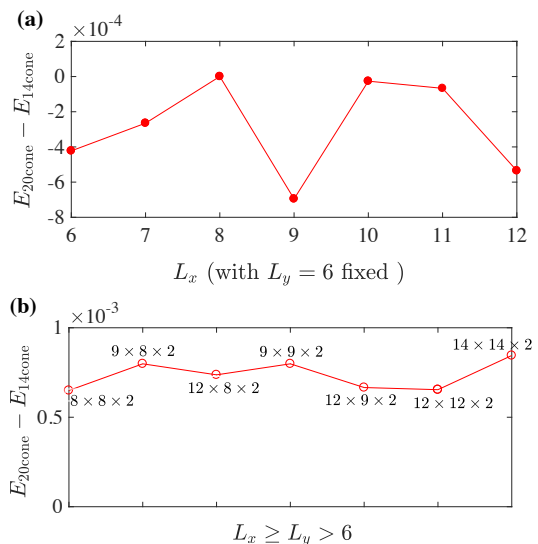


FIG. S3. (a) Energy difference per site between the 20-cone and 14-cone states in VMC calculations for systems with short dimension  $L_y = 6$ , where the 20-state lies lower in energy. (b) Energy difference for system sizes  $L_x \times L_y \times 2$  with  $L_x \geq L_y > 6$ , where the 14-cone state is lower in energy.

where the cylinder circumference is fixed to  $L_y = 3$  unit cells while its length is  $L_x = 18, 24$ , and  $30$ . As shown in Figs. S2(a), S2(b), and S2(c), indeed we find a very broad regime of QSL phases whose width increases with  $L_x$ , limiting the ordered (IS) phase to values only beyond  $\Gamma/|K| = 3$  on long cylinders.

When the circumference is increased to  $L_y = 6$  (system size  $12 \times 6 \times 2$  sites), we find a zigzag-ordered phase for all parameter ratios  $\Gamma/|K| > 0.9$ , which is absent when  $L_y = 3$  [Fig. S2(d)]. Further, a ferromagnetic phase appears at small  $\Gamma$ , separating the KSL from the analog of the PKSL for this geometry (because of the finite number of  $\mathbf{k}$  values in the transverse direction, this magnetically disordered state will not have the full complement of gapless cones). This result alone demonstrates that the  $K$ - $\Gamma$  model on the honeycomb lattice is subject to very strong finite-size effects, and that conclusions in favor of QSL states at large  $\Gamma$  are artifacts of the system sizes considered.

Further investigation reveals, however, that the  $L_y = 6$  geometry is still anomalous, especially in the PKSL regime. In our VMC calculations for the  $12 \times 6 \times 2$  system we find that the ground state in the intermediate regime  $0.23 < \Gamma/|K| < 0.55$  is a gapless  $Z_2$  QSL corresponding in the 2D system to the 20-cone state. This competes with the 14-cone state, whose energy is higher by values ranging from 0 to  $7 \times 10^{-4}|K|$ , as shown in Fig. S3(a). However, for all larger accessible system sizes with  $L_x \geq L_y > 6$ , these conditions are reversed and the 14-cone state becomes lower in energy, as detailed in Fig. S3(b). Although our system sizes preclude a reliable extrapolation to the thermodynamic limit, by calculations on systems up to  $14 \times 14 \times 2$  we infer that the ground state in this limit is indeed the 14-cone PKSL phase, and

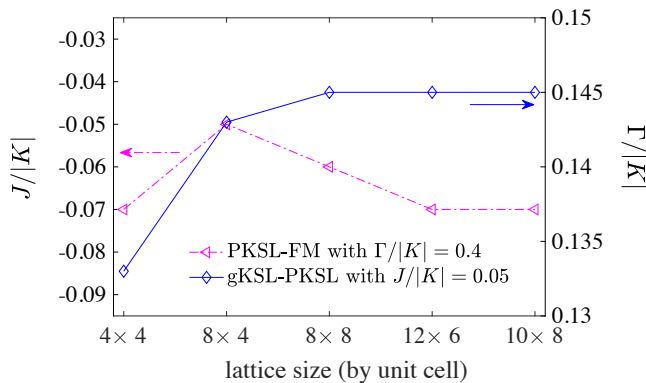


FIG. S4. Dependence on system size of the phase boundary between the gKSL and PKSL phases, computed at fixed  $J/|K| = 0.05$ , and of the boundary between the PKSL phase and the FM ordered phase, computed at fixed  $\Gamma/|K| = 0.4$ .

that the 20-cone ground state is an artifact of the  $L_y = 6$  geometry. Here we comment that the energies we calculate for the  $12 \times 12 \times 2$  and  $14 \times 14 \times 2$  geometries are not obtained variationally, but are computed using the variational parameters of the same states on the  $12 \times 8 \times 2$  cluster. From these smaller systems we find that changes to the variational parameters are negligible when compared to changes due to the cluster geometry, and hence we infer that the large-system energies are reliable.

In view of all of these complexities, we performed a large number of studies to ensure that the phase diagram presented in Fig. 1 of the main text is completely reliable. To eliminate finite-size effects to the best of our ability, we determined every point in the phase diagram by examining its evolution with system size. We illustrate the results of these investigations in Fig. S4, where we show the size-dependence of the phase boundary in two cases. For the transition from a QSL (the PKSL) to an ordered state (the FM phase), we find rather little variation even from small sizes; for the transition of most interest to the present study, that from the gKSL to the PKSL phase, we find that a stable limiting value does require system sizes large in both dimensions.

## S5. DYNAMICAL STRUCTURE FACTOR

To understand the nature of the PKSL, we deduce its physical properties and contrast them with those of the gKSL, which is also a gapless QSL. To this end we investigate the magnetic response in the form of the dynamical structure factor (DSF),  $S^{mn}(\mathbf{q}, \omega)$  ( $m, n = x, y, z$ ), which we compute at the level of linear response. From the fluctuation-dissipation theorem, the DSF is defined by

$$S^{mn}(\mathbf{q}, \omega) = -\frac{1}{\pi} [1 + n_B(\omega)] \chi''^{mn}(\mathbf{q}, \omega), \quad (\text{S19})$$

where  $n_B(\omega)$  is the Bose-Einstein distribution and  $\chi''^{mn}(\mathbf{q}, \omega) = \lim_{\delta \rightarrow 0} \text{Im} \chi^{mn}(\mathbf{q}, \omega + i\delta)$  is the imag-

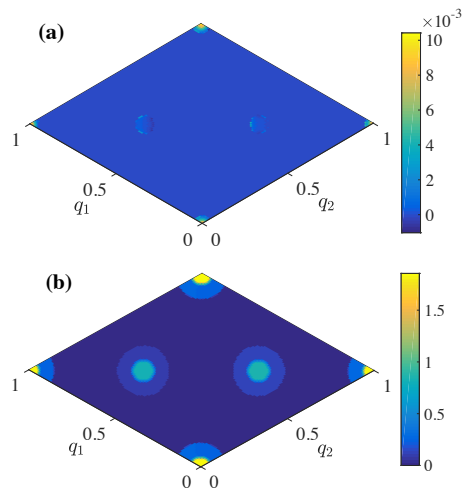


FIG. S5. Dynamical structure factor illustrated for the gKSL ( $\Gamma/|K| = 0.1$ ,  $J/|K| = 0.05$ ).  $\omega_0 = 0.082|K|$  is the minimum energy of the gapped,  $b^m$ -dominated spinon bands. (a) Sum over all frequencies  $\omega \leq \omega_0$ . (b) Sum over frequencies  $\omega_0 \leq \omega \leq \omega_0 + 0.018|K|$ . Note the logarithmic intensity scale.

inary part of the analytic continuation of the finite-temperature susceptibility,  $\chi^{mn}(\mathbf{q}, i\omega)$ . To interpret the low-energy spin response of the PKSL, it is most convenient to express the DSF in the Majorana representation of Eq. (S1). As an example, we illustrate the processes contributing to  $\chi^{zz}(\mathbf{q}, i\omega)$  in the form

$$\begin{aligned} \chi^{zz}(\mathbf{q}, i\omega) &= \int_0^\beta \langle T_\tau S_{\mathbf{q}}^z(\tau) S_{-\mathbf{q}}^z(0) \rangle e^{i\omega\tau} d\tau \\ &= - \int_0^\beta \sum_{\mathbf{k}\mathbf{p}} \langle T_\tau c_{-\mathbf{k}}(\tau) b_{\mathbf{k}+\mathbf{q}}^z(\tau) c_{-\mathbf{p}}(0) b_{\mathbf{p}-\mathbf{q}}^z(0) \rangle e^{i\omega\tau} d\tau \\ &= \int_0^\beta \sum_{\mathbf{k}} [\langle T_\tau c_{-\mathbf{k}}(\tau) c_{\mathbf{k}}(0) \rangle \langle b_{\mathbf{k}+\mathbf{q}}^z(\tau) b_{-\mathbf{k}-\mathbf{q}}^z(0) \rangle \\ &\quad - \langle T_\tau c_{-\mathbf{k}}(\tau) b_{\mathbf{k}}^z(0) \rangle \langle b_{\mathbf{k}+\mathbf{q}}^z(\tau) c_{-\mathbf{k}-\mathbf{q}}(0) \rangle] e^{i\omega\tau} d\tau, \end{aligned}$$

where  $T_\tau$  denotes time-ordering and  $\langle \dots \rangle$  the thermal average (which at zero temperature is equivalent to averaging over the mean-field ground state). It is clear that processes contributing to the DSF involve the excitation of two Majorana fermions created by a  $c$  and a  $b^z$  operator, with total momentum  $\mathbf{q}$  and total energy  $\omega$ . At low energies, the DSF will be nonzero if one or both of the following two situations is/are satisfied: (a) both the  $c$  and the  $b^z$  fermions are gapless; (b) the  $c$  and  $b^z$  fermions are hybridized at the nodal points of the PKSL dispersion.

In the KSL ( $J = 0 = \Gamma$ ), the  $c$  fermions are gapless and independence of the four species is a defining property, hence neither (a) nor (b) is applicable and the spin response is gapped. In the gKSL, the  $b^m$ -dominated bands retain a robust gap, which we label  $\omega_0$  and which precludes case (a). In Ref. [2] it was argued qualitatively, on the basis of symmetry and gauge constraints, that the system remains gapped when  $J = 0$  or  $\Gamma = 0$ ,

$\frac{\Gamma}{ K }$	$\frac{J}{ K }$	Cone	$ \langle c_{\mathbf{k}}   \gamma_{\mathbf{k}} \rangle ^2$	$ \langle b_{\mathbf{k}}^x   \gamma_{\mathbf{k}} \rangle ^2$	$ \langle b_{\mathbf{k}}^y   \gamma_{\mathbf{k}} \rangle ^2$	$ \langle b_{\mathbf{k}}^z   \gamma_{\mathbf{k}} \rangle ^2$
0	0.1	K	1	0	0	0
0.1	0.0	K	1	0	0	0
	0.05	K	0.9997	$1.04 \times 10^{-4}$	$1.04 \times 10^{-4}$	$1.04 \times 10^{-4}$
0.3	0.0	K	0.3616	0.2128	0.2128	0.2128
		K <sub>1</sub>	0.1850	0.4009	0.4009	0.0133
		K <sub>2</sub>	0.2528	0.0717	0.0717	0.6038

TABLE S1. Projected weights of Majorana fermions at the gapless momentum points in selected gKSL and PKSL phases when expressed in terms of the  $c$ ,  $b^x$ ,  $b^y$ , and  $b^z$  fermions [Eq. (S1)]. K<sub>1</sub> and K<sub>2</sub> denote the first two blue points from left to right in Fig. 2(d) of the main text.

but that the generic spin response is gapless. It is for this reason that we distinguish between the KSL and the gKSL. In our spinon representation, the nature of this case (b) gapless response is quantified through the  $c$ - $b^m$  hybridization, which we compute at  $\omega \rightarrow 0$  by projecting the eigenstates we obtain onto the  $\{c, b^x, b^y, b^z\}$  basis. The results are shown in Table S1: for the parameter sets ( $\Gamma/|K| = 0.1$ ,  $J = 0$ ) and ( $\Gamma = 0$ ,  $J/|K| = 0.1$ ), the ground states we find are those with  $\eta_3 = 0$  and  $\eta_5 = 0$ , ensuring that hybridization is completely absent; by contrast, for ( $\Gamma/|K| = 0.1$ ,  $J/|K| = 0.05$ ) the optimized values of  $\eta_3$  and  $\eta_5$  are nonzero but remain small [ $O(10^{-2})$ ], as a result of which the hybridization is very weak [ $O(10^{-4})$ ]. The corresponding DSF, shown in Figs. S5(a) and S5(b), remains strongly suppressed until finite energies  $\omega \approx \omega_0$ . Thus although the gKSL has a gapless spin response when both  $J$  and  $\Gamma$  are finite, in practice the degree of hybridization remains small out to the first-order transitions terminating its phase space, and hence the DSF may be very small at frequencies  $\omega < \omega_0$ . This situation could result in the erroneous identification of a gapped QSL in inelastic neutron scattering experiments, which cannot access the lowest energy scales, and may require nuclear magnetic or electron spin resonance (NMR or ESR) measurements to identify the gapless nature. We comment that the mean-field band gap of the  $b^m$  fermions we compute is larger than the true flux-excitation gap, as pointed out by Kitaev [8], and thus the mean-field DSF provides only a qualitative reflection of the spin response, but not a quantitative statement of the value  $\omega_0$  that governs it.

In the PKSL, the projected weights shown in Table S1 demonstrate clearly that all of the eigenstates are strongly hybridized superpositions of all four basis states, at all of the cones and even as  $\omega \rightarrow 0$ . Thus both (a) and (b) are relevant. The low-energy DSF shown in Fig. 2(e) of the main text is a consequence of two-cone processes involving any of the 14 cones, with different weights for each different type of intra- or intercone pair. When the energy increases towards the width of the lowest band, the DSF is no longer controlled by the nodal points and becomes continuous across the Brillouin zone, as shown in Fig. 2(f) of the main text. At all energies the DSF is strongest at  $\mathbf{q} = 0$ , and indeed we note that the peaks in

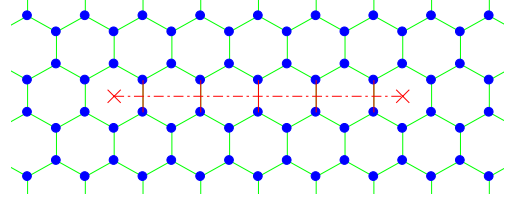


FIG. S6. Two vortices inserted at the hexagons marked by red crosses define a branch cut (dot-dashed line).

Fig. 2(e) of the main text have been cut from an intensity of 16 to 6 in order to show the structure of the low-energy DSF more clearly throughout the Brillouin zone.

## S6. FIELD-INDUCED TOPOLOGICAL STATES

As we have shown in the main text, the PKSL in an applied magnetic field  $\mathbf{B} \parallel \hat{c}$  provides examples of the  $\nu = 5$  and  $\nu = 4$  chiral spin-liquid (CSL) states of Ref. [8]. While high- $\nu$  CSL phases have been studied in  $SO(n)$ -symmetric [9, 10] and spin  $S > 1/2$  systems [11, 12], here we have realized them in a  $S = 1/2$  lattice model with only short-range interactions. In an in-plane field  $\mathbf{B} \parallel (\mathbf{x} - \mathbf{y})$ , the gapless 14-cone state is preserved for small but finite field strengths. The phase diagrams as a function of  $|\mathbf{B}|$  are shown in Fig. 3 of the main text and here we provide the results supporting our conclusions.

To perform VMC calculations in a magnetic field, we add the Zeeman-coupling term,

$$H_{\text{Zeeman}} = g\mu_B \mathbf{B} \cdot \frac{1}{2} C_i^\dagger \boldsymbol{\sigma} C_i,$$

to the mean-field Hamiltonian and reoptimize the parameters under Gutzwiller projection. For convenience we introduce the normalized field strength  $\tilde{B} = g\mu_B B/|K|$ . As in Ref. [1], we assume an uniform and isotropic  $g$ -factor for all field directions. To investigate the physics of anyons in the CSL phases, we introduce a pair of vortices in the system, as represented in Fig. S6, by reversing the signs of the mean-field terms on the bonds intersected by the dot-dashed line.

### A. $\mathbf{B} \parallel \mathbf{c}$

In the gKSL for  $K < 0$ , there is a single phase transition with increasing the field strength [13]. For  $\tilde{B} < \tilde{B}_c$  ( $= 0.19$  for  $\Gamma/|K| = 0.1$ ,  $J = 0$ ), the mean-field dispersion is fully gapped, this gap growing linearly with  $|\tilde{B}|$  when  $|\tilde{B}|$  is small, except when  $J = 0$  or  $\Gamma = 0$ , in which case it is proportional to  $|\tilde{B}|^3$ . The ground state has Chern number  $\nu = 1$ , so one Majorana zero mode is bound to each vortex,  $\sigma$ , and the vortices obey the well-known fusion rule  $\sigma \times \sigma = 1 + \varepsilon$ , where 1 is the vacuum and  $\varepsilon$  is a fermion. 1,  $\varepsilon$ , and  $\sigma$  are the three topologically distinct sectors in the system, as shown in Table I of the main text, and correspond to the GSD of 3.

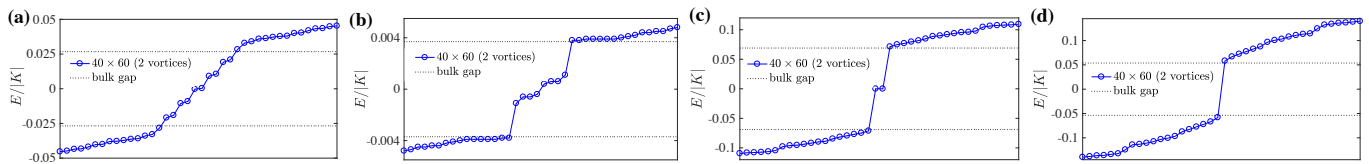


FIG. S7. Energy spectrum of the mean-field Hamiltonian in the vicinity of the gap, computed for a large system in four different external magnetic fields  $\mathbf{B} \parallel \mathbf{c}$  and in the presence of two vortices (Fig. S6). The interaction parameters are those of the PKSL ( $\Gamma = 0.3|K|$ ,  $J = 0$ ) and the mean-field parameters are determined by VMC calculations with system size  $8 \times 8 \times 2$ . (a)  $\tilde{B}_x = 0.1$ , where each vortex binds two complex fermion modes plus a Majorana zero mode ( $\nu = 5$ ); (b)  $\tilde{B}_x = 0.4$ , where each vortex binds two mid-gap complex fermion modes ( $\nu = 4$ ); (c)  $\tilde{B}_x = 0.5$ , where each vortex binds a Majorana zero mode ( $\nu = 1$ ; this state becomes trivial after Gutzwiller projection); (d)  $\tilde{B}_x = 0.85$ , where no mid-gap modes are trapped by the vortex.

To show this we apply the following considerations. A fermion experiences a flux  $\pi$  on moving around a vortex, whence the vortices appear in pairs. A pair of  $\pi$ -fluxes gives rise to two Majorana zero modes, equivalent to a single fermion mode, whose energies fall in the bulk gap [similar to Fig. S7(c)]. Because of the nonzero Chern number, each vortex ( $\sigma$ ) is associated with a gauge charge  $1/4$ , a situation analogous to the Hall effect [14]. When two vortices are exchanged, the Aharonov-Bohm phase between the  $\pi$ -flux and the associated charge is counted only once. Thus the topological spin (the Abelian phase obtained by rotating a vortex by  $2\pi$ , which by the spin-statistics theorem is the same as the phase obtained by exchanging two vortices) is equal to  $e^{i\frac{\pi}{4} \times \frac{1}{2}} = e^{i\frac{\pi}{8}}$ .

If a fermion, which has gauge charge  $-1$  [8], is attached to a vortex, the composite vortex  $\sigma \times \varepsilon$  also has topological spin  $e^{i\frac{\pi}{8}}$ : exchanging two composite vortices creates a phase  $e^{i(\frac{\pi}{8} - \frac{\pi}{2} - \frac{\pi}{2} + \pi)}$ , where the factors of  $e^{-i\frac{\pi}{2}}$  arise from the fermion and  $\pi$ -flux moving half a circle around each other and the phase  $e^{i\pi}$  from the exchange of two fermions. In fact a composite vortex has the same properties as a vortex (except for the gauge charge, which is not measurable), resulting in the fusion rule  $\sigma \times \varepsilon = \sigma$  [8], confirming that the set of three topologically distinct sectors is closed.

After Gutzwiller projection, if it remains  $Z_2$ -deconfined then the  $\nu = 1$  mean-field state becomes a non-Abelian CSL, in which the vortices are Ising anyons. Our VMC calculations for the gKSL in a field verify that the GSD of this CSL on a torus is 3, as stated in Sec. S2 for any system with an odd Chern number. When  $\tilde{B} > \tilde{B}_c$ , the projected state is  $Z_2$ -confined and the GSD is 1, i.e. the system enters a topologically trivial gapped phase, which is connected adiabatically to the fully polarized state.

Turning to the PKSL, one may apply all of the same considerations. We find that there are two phase transitions, which for  $\Gamma/|K| = 0.3$ , occur at  $\tilde{B}_1 = 0.28$  and  $\tilde{B}_2 = 0.71$ . When  $\tilde{B} < \tilde{B}_1$ , the Chern number is  $\nu = 5$ : the vortex carries gauge charge  $\nu/4 = 5/4$ , which give rise to a topological spin  $e^{i\frac{5}{8}\pi}$ . One vortex traps two complex fermion modes plus one unpaired Majorana zero mode, as shown in Fig. S7(a) by computing the low-energy spectrum at the mean-field level for a large system. The odd Chern number means that the vortex is a non-Abelian

anyon and correspondingly the  $\nu = 5$  phase is a non-Abelian CSL. This nontrivial topological order is verified in VMC by the three-fold degeneracy of the ground state on a torus, as shown by the eigenvalues of the density matrix listed in Table S2. Despite their commonalities, the  $\nu = 1$  and  $\nu = 5$  phases differ in the topological spin of their vortices, their total chiral central charge, and their thermal Hall conductance (Table I of the main text).

When  $\tilde{B}_1 < \tilde{B} < \tilde{B}_2$ , the Chern number is  $\nu = 4$ . As shown in Fig. S7(b), a pair of vortices gives rise to four mid-gap fermion modes, whose energies are nonzero. In principle each vortex (denote by  $m$  [8]) traps four Majorana zero modes, but these lower their energies by coupling to form two complex fermion modes. Thus the vortex,  $m$ , carries gauge charge  $\nu/4 = 1$  and has topological spin  $e^{i\frac{\pi}{2} \times 1} = e^{i\frac{\pi}{2}}$ , meaning that it is a semion. The composite object of two  $m$  vortices has statistical angle  $\pi/2 \times 4 = 2\pi$ , which means it is a boson ( $m \times m = 1$ ).

The attachment of a fermion,  $\varepsilon$ , to the vortex creates a new composite vortex,  $m \times \varepsilon = e$ . Similar to the previous discussion, this does not change the topological spin, i.e.  $e$  is also a semion, with  $e \times e = 1$ . Thus it is easy to obtain the remaining fusion rules,  $e \times m = \varepsilon$ ,  $e \times \varepsilon = m$ , and  $m \times \varepsilon = e$ . The nontrivial topological order of the projected  $\nu = 4$  state is reflected by the GSD on a torus, which is 4 (Table S2).

For  $\tilde{B} > \tilde{B}_2$ , the outcome of VMC is a trivial, gapped,  $Z_2$ -confined phase. However, working at the mean-field level (with the parameters determined from VMC), there is an additional critical point at  $\tilde{B}_3 \sim 1.22$  where the mean-field Chern number changes from  $\nu = 1$  to  $\nu = 0$ .

$\tilde{B}_x$	$\nu$	$\rho_1$	$\rho_2$	$\rho_3$	$(\rho_4)$	GSD
0.1	5	0.4016	0.8456	1.7527		3
0.4	4	0.7506	0.8168	0.8303	1.6024	4
0.5	1	$8.0 \times 10^{-6}$	$7.6 \times 10^{-4}$	2.9992		1
0.85	0	$7.5 \times 10^{-9}$	$3.0 \times 10^{-7}$	$5.6 \times 10^{-6}$	4.0000	1

TABLE S2. Eigenvalues of the density matrices of the CSL ground states induced by a magnetic field  $\mathbf{B} \parallel \hat{c}$ , computed in the PKSL ( $\Gamma/|K| = 0.3$ ,  $J = 0$ ) for a system of size  $8 \times 8 \times 2$ .  $\nu$  is the mean-field Chern number; as discussed in the text, the projected  $\nu = 1$  and  $\nu = 0$  states are the same phase.

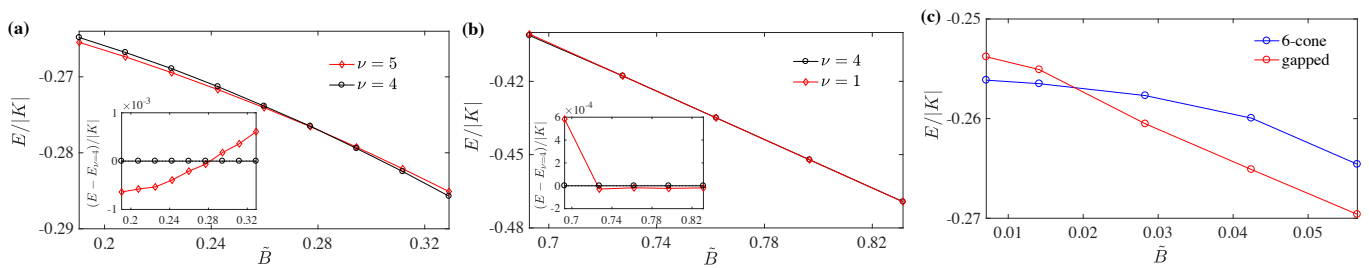


FIG. S8. Field-induced phase transitions in the PKSL ( $\Gamma/|K| = 0.3$ ,  $J = 0$ ). (a) Level-crossing at the transition from the  $\nu = 5$  to the  $\nu = 4$  CSL in a field  $\mathbf{B} \parallel \mathbf{c}$  and (b) level-crossing at the transition from the  $\nu = 4$  CSL, which is  $Z_2$ -deconfined, to the trivial ( $Z_2$ -confined) phase obtained by projection of the  $\nu = 1$  mean-field state. Both insets show the energy difference per site with respect to the  $\nu = 4$  state. (c) Level-crossing from the gapless 6-cone state to a trivial gapped phase in a field  $\mathbf{B} \parallel (\mathbf{x} - \mathbf{y})$ .

The number of mid-gap states in the mean-field spectrum changes correspondingly from 2 [Fig. S7(c)] to 0 [Fig. S7(d)]. However, as Table S2 shows clearly, both the projected  $\nu = 1$  state and the projected  $\nu = 0$  state have a GSD of 1, showing that they are  $Z_2$ -confined. Usually, a mean-field state with nontrivial Chern number is nontrivial after Gutzwiller projection, but in the present case our numerical results indicate that the strong magnetic field causes the highly polarized projected state to become  $Z_2$ -confined. This confinement can be interpreted as a closing of the  $Z_2$  vison gap despite the fact that the mean-field spinon gap is still finite. We comment in closing this subsection that the transitions at both  $\tilde{B}_1$  and  $\tilde{B}_2$  are first-order, as shown in Figs. S8(a) and S8(b), and hence the closure of the spinon gap required at a continuous topological transition is absent.

### B. $\mathbf{B} \parallel (\mathbf{x} - \mathbf{y})$

Here we discuss only the PKSL. An in-plane magnetic field breaks the three-fold rotation symmetry and in general a gap will be opened at all the cones. However, as noted in the main text, for the special directions  $\mathbf{B} \parallel (\mathbf{x} - \mathbf{y})$ ,  $(\mathbf{y} - \mathbf{z})$ , and  $(\mathbf{z} - \mathbf{x})$ , 6 of the cones remain gapless at small but finite fields. As the field is increased, pairs of cones move together and may merge,

then become gapped at a second-order phase transition [1]. In the PKSL, a first-order transition preempts this process, as shown in Fig. S8(c), and instead the system enters a phase whose GSD on a torus is 1, meaning that it is  $Z_2$ -confined and trivial. We find that this state, which is connected directly to the fully polarized limit, is characterized by strong spatial anisotropy and a sign-reversal of the variational parameter  $\rho_a$ . All of the first-order transitions in Fig. S8 reinforce the observation that many states compete strongly at low energies, which in turn raises the computational complexity of the task of deducing the full phase diagram in  $K$ ,  $J$ ,  $\Gamma$ ,  $|\mathbf{B}|$ , and  $\hat{B}$ .

### C. General $\mathbf{B}$

Before concluding this section, we provide one brief illustration of the possibilities that arise when applying the magnetic field in an intermediate direction, and when applying it to an ordered phase. For a field orientation fixed along the direction  $[1, 1, 0.2]$  and interaction parameters fixed at  $(\Gamma/|K| = 1.4, J = 0)$  [1], we observe a phase transition at  $\tilde{B} = 0.36$  from the zigzag phase to a  $\nu = 1$  CSL. This CSL phase is stable in the field range  $0.36 < \tilde{B} < 0.50$ . It supports a half-quantized thermal Hall conductance, a result which may be of key importance in interpreting the results of experiments such as that reported in Ref. [15].

- 
- [1] Z.-X. Liu and B. Normand, Phys. Rev. Lett. **120**, 187201 (2018).
  - [2] X.-Y. Song, Y.-Z. You, and L. Balents, Phys. Rev. Lett. **117**, 037209 (2016).
  - [3] Y.-Z. You, I. Kimchi, and A. Vishwanath, Phys. Rev. B **86**, 085145 (2012).
  - [4] A. Kitaev, AIP Conf. Proc. **1134**, 22 (2009).
  - [5] X.-G. Wen, Phys. Rev. B **85**, 085103 (2012).
  - [6] J. G. Rau, E. K.-H. Lee, and H.-Y. Kee, Phys. Rev. Lett. **112**, 077204 (2014).
  - [7] M. Gohlke, G. Wachtel, Y. Yamaji, F. Pollmann, and Y. B. Kim, Phys. Rev. B **97**, 075126 (2018).
  - [8] A. Kitaev, Ann. Phys. **321**, 2 (2006).
  - [9] H.-H. Tu, Phys. Rev. B **87**, 041103 (2013).
  - [10] S. Yang, T. B. Wahl, H.-H. Tu, N. Schuch, and J. I. Cirac, Phys. Rev. Lett. **114**, 106803 (2015).
  - [11] M. Greiter and R. Thomale, Phys. Rev. Lett. **102**, 207203 (2009).
  - [12] Z.-X. Liu, H.-H. Tu, Y.-H. Wu, R.-Q. He, X.-J. Liu, Y. Zhou, and T.-K. Ng, Phys. Rev. B **97**, 195158 (2018).
  - [13] H.-C. Jiang, Z.-C. Gu, X.-L. Qi, and S. Trebst, Phys. Rev. B **83**, 245104 (2011).
  - [14] C. Nayak, S. H. Simon, A. Stern, M. Freedman, and S. Das Sarma, Rev. Mod. Phys. **80**, 1083 (2008).
  - [15] Y. Kasahara, T. Ohnishi, Y. Mizukami, O. Tanaka, S. Ma, K. Sugii, N. Kurita, H. Tanaka, J. Nasu, Y. Motome,

T. Shibauchi, and Y. Matsuda, *Nature* **559**, 227 (2018).